Soil Dynamics and Earthquake Engineering 113 (2018) 215–229

Contents lists available at ScienceDirect

Soil Dynamics and Earthquake Engineering

journal homepage: www.elsevier.com/locate/soildyn

Effect of geometry on in-plane responses of a symmetric canyon subjected by *P* waves

Wen-Shinn Shyu[a], Tsung-Jen Teng[b], Chuen-Shii Chou[c,*]

[a] Department of Civil Engineering, National Pingtung University of Science and Technology, Pingtung, Taiwan, ROC
[b] National Center for Research on Earthquake Engineering, Taipei, Taiwan, ROC
[c] Department of Mechanical Engineering, National Pingtung University of Science and Technology, Pingtung, Taiwan, ROC

ARTICLE INFO

Keywords:
P wave
Canyon
Hybrid method
Transfinite interpolation
Site effects

ABSTRACT

Topographic site effects in anti-plane problems have been studied for four decades cause of the obtained analytical solutions. The authors have developed proposed hybrid methods combining Lamb's series with finite element method (FEM) to resolve the problem of anti-plane scattering; however, it has been difficult to account for site effects in in-plane problems due to mode conversion. In this study, we sought to resolve this issue by developing a novel hybrid method to investigate the site effects of a canyon subjected to longitudinal waves (*P* waves) as well as horizontal and vertical displacement amplitudes ($|u_x|$ and $|u_z|$) near and along canyons of various shapes. A transfinite interpolation function (TFI) was used to obtain the coordinates of nodes and conduct node numbering in the inner finite region within the canyon. Combining hybrid method with TFI function, similar procedures can be used to resolve the scattering problems in both anti-plane and in-plane problems.

Canyons are divided into three groups according to shape: 1) smooth shallow, 2) non-smooth, and 3) smooth deep. We also examine the incident angle of *P* waves (θ), the dimensionless frequencies (η), and the shape of a canyon in terms of their effect on $|u_x|$ and $|u_z|$. These factors were shown to generate site effects, including canyon-decay-effect, oblique-effect, shield effect, and SDCP (slope discontinuous points) effect. The site effects induce variations in $|u_x|$ and $|u_z|$ with constructive interference in the illuminated zone, destructive interference in the shadow zone, and attenuation along the surface of the canyon.

1. Introduction

Site effects due to surface irregularities can result in the enlargement and/or suppression of ground motion at the free surface. This can be attributed to the scattering and diffraction of propagating waves. Site effects are important in the erection of structures, such as bridges across canyon, wherein the peak ground acceleration values vary considerably between the bottom of the canyon and the upper corners [1]. Therefore, the problem of wave propagation in a canyon subjected to anti-plane waves (*SH* waves) for decades, which are uncoupled from other planar waves, has been studied by simplifying the geometric shapes of the irregularities and specifying the source of the waves. The governing equation can be solved using the separation of variables method, which means that the anti-plane problem can be solved analytically. The separation of variables approach can be applied to orthogonal coordinates [2] to derive the wave function expansion method (WFEM), by which the Bessel functions as standing waves and Hankel functions as outgoing waves are incorporated in a cylindrical coordinate system.

The boundary condition of in-plane problems (traction free at the free surface) stipulates that incident longitudinal waves (*P* waves) or transverse waves (*SV* waves) cause mode conversion [3] during the reflection of waves at the half-plane surface. The complexity of the governing equation of in-plane problems means that the separation of variables method is insufficient to resolve the problem of in-plane scattering using basis functions in the orthogonal coordinates. This led to the application of various numerical methods to resolve the problem of in-plane scattering: boundary element method (BEM) based on the exact Green's function for an irregular topographic feature in an elastic half-space [4], the weighted residual method for 2-D canyons of arbitrary shape [5] and an almost circular arbitrary-shaped canyon [6]. A complicated series (such as Lamb's series) has been used to provide a quasi-analytical solution to the problem of in-plane scattering. Wong combined the generalized inverse method with a trial function based on the Lamb's series to characterize wave propagation by a semi-elliptical canyon [7]. Yeh et al. combined BEM with Lamb's series to solve the

* Corresponding author.
E-mail address: cschou@mail.npust.edu.tw (C.-S. Chou).

https://doi.org/10.1016/j.soildyn.2018.06.003
Received 4 January 2018; Received in revised form 22 April 2018; Accepted 3 June 2018
0267-7261/

problem of in-plane scattering [8]. Yeh et al. also used the Lamb's series as a set of scattering basis functions to solve the problem of in-plane scattering by semi-cylindrical canyons [9]; however, the series produces standing waves, which hinder precise via numerical methods. Cao and Lee [10] and Yang [11] treated the half-plane as a circular boundary of large radius when using WFEM to resolve the problem of in-plane scattering in a circular-arc canyon. Lee and Liu proposed a stress-free wave function to solve a two-dimensional scattering and diffraction of *P*- and *SV*- waves along a semi-circular canyon in an elastic half-space. They claim to have found closed-form analytic solutions to the problem [12], based on the assumption that the straight free surface of the half-space was replaced using a circular-arc boundary with a large radius.

Our motivation in this study was to resolve the problem of *P* wave scattering by a canyon through extending the proposed hybrid method combining finite element method (FEM) with a Lamb's series [13,14]. The geometry of a canyon meshed using transfinite interpolation (TFI) [15] and the mass matrix as well as stiffness matrix based on FEM are applicable to anti-plane as well as in-plane problems. Hence, a suitable Lamb's series satisfying the in-plane problem was needed to introduce for our hybrid method. This means the proposed hybrid method based on functional could be used to resolve the problem of scattering in space with modifying the governing equations as well as the boundary conditions.

In this paper, we examine the displacement patterns of the following five typical canyons: circular-are shape (two examples, including a very shallow canyon), semi-circular, trapezoidal, triangular, and semi-elliptical (two examples, including a very deep canyon). The hybrid method eliminates the influence of irregularities in the geometry and the types of incident wave (e.g., body waves or surface waves). This strategy has previously been used to resolve the problem of *SH* wave scattering in an oblique-truncated semicircular canyon [16], a partially filled alluvial valley [17], and a trapezoidal dike [18]. Considering the body waves, though *P* waves carry less energy than do secondary (*SV*) waves; however, they are the "primary waves" with a velocity faster than *SV* waves. The characterization of *P* waves associated with canyons of various shapes may be helpful in the prediction of earthquakes, with the period between the arrival of *P* waves and *SV* waves providing a window in which to prepare. In other words, the results obtained in this study could be used in the development of an early warning system for earthquakes in the future.

The hybrid method proposed in this paper is applicable to the problem of in-plane scattering, and can also be used in conjunction with TFI to mesh canyons of various shapes. We compared our numerical results involving semi-circular canyons with those reported by Yeh et al. [9]. We also divided canyons into three groups based on their shape to investigate the site effects of canyons on vertical and horizontal displacements (in the frequency domain) at the surface and in areas surrounding the canyon.

2. Numerical model

2.1. A half-space impinged by incident P waves

Fig. 1 presents a schematic illustration showing an elastic half-space on the *x*-*z* plane excited by *P* waves with circular frequency (ω) and incident angle (θ). The generated wave speeds and wave numbers are given by:

$$C_p = \sqrt{\frac{\lambda + 2\mu}{\rho}};\ C_s = \sqrt{\frac{\mu}{\rho}} \tag{1a}$$

$$k_p = \frac{\omega}{C_p};\ k_s = \frac{\omega}{C_s} \tag{1b}$$

where ρ represents the density; λ and μ represent the Lamé constants in the elastic half-space; C_p and C_s respectively represent the

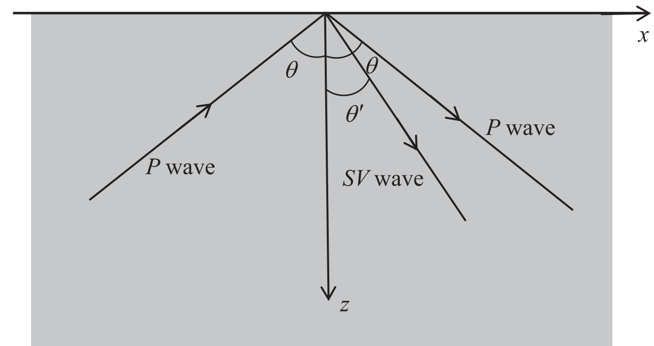

Fig. 1. Schematic diagram showing an elastic half-space excited by *P* waves.

speeds of *P* waves and *SV* waves; and symbols k_p and k_s respectively represent the wave numbers of *P* waves and *SV* waves. By disregarding the effects of ω, the potential form of incident *P* waves is given by the following:

$$\phi^{\mathrm{i}} = Ae^{-i(\xi x - \alpha z)} \tag{2}$$

where $i = \sqrt{-1}$, and ϕ^{i} represents the incident potential of *P* waves with an amplitude of $A = \frac{1}{k_p}$. The incident apparent *P* wave number (ξ) is expressed using $\xi = k_p \sin\theta = k_s \sin\theta'$, which results in $\theta' = \sin^{-1}\left(\frac{C_s}{C_p}\sin\theta\right)$. The reflected apparent *P* and *SV* wave numbers are $\alpha = k_p \cos\theta$ and $\beta = k_s \cos\theta'$, respectively. The angle of reflected *P* waves is the same as incident angle θ, and the angle of reflected *SV* waves is defined as θ', as shown in Fig. 1. Thus, the potential forms of the reflected *P* waves (ϕ^{r}) and *SV* waves (ψ^{r}) are given as follows:

$$\phi^{\mathrm{r}} = A_p e^{-i(\xi x + \alpha z)};\ \psi^{\mathrm{r}} = A_s e^{-i(\xi x + \beta z)} \tag{3}$$

where A_p and A_s are amplitudes determined by the traction free conditions imposed by the free half-space. The ratios of $\frac{A_p}{A}$ and $\frac{A_s}{A}$ are respectively given as follows:

$$\frac{A_p}{A} = \frac{\sin 2\theta \sin 2\theta' - \kappa^2 \cos^2 2\theta'}{\sin 2\theta \sin 2\theta' + \kappa^2 \cos^2 2\theta'};\ \frac{A_s}{A} = \frac{-2\sin 2\theta \cos 2\theta'}{\sin 2\theta \sin 2\theta' + \kappa^2 \cos^2 2\theta'};\ \kappa = \frac{k_s}{k_p} \tag{4}$$

The displacements in the free field ($\mathbf{u}^f = (u_x^f, u_z^f)$) produced by the combined effects of incident *P* waves and the reflected *P* and *SV* waves can be expressed in the following complex form:

$$u_x^f = -i\xi(\phi^{\mathrm{i}} + \phi^{\mathrm{r}}) + i\beta\psi^{\mathrm{r}};\ u_z^f = i\alpha(\phi^{\mathrm{i}} - \phi^{\mathrm{r}}) - i\xi\psi^{\mathrm{r}} \tag{5}$$

We assumed the parameters of the half-space, which included a Poisson's ratio equal to $\frac{1}{3}$, $\mu = 1.0$, and $\rho = 1.0$, such that $C_s = 1.0$ and $\frac{C_p}{C_s} = 2.0$. Variations in the absolute values of u_x^f and u_z^f at the free surface (i.e., $|u_x^f(x, 0)|$ and $|u_z^f(x, 0)|$) associated with θ are shown in Fig. 2 and Table 1. The results in Fig. 2 reveal the following interesting findings. (1) When $\theta = 0$, only $|u_z^f(x, 0)|$ is observed at the free surface. (2) An increase in θ from 0 to $\pi/2$ leads to a decrease in $|u_z^f(x, 0)|$ from its maximum value to zero; however, $|u_x^f(x, 0)|$ increases from 0 to its maximum value when θ approaches a critical angle (such as $\pi/3$), whereupon the value of $|u_x^f(x, 0)|$ decays to 0. For this reason, we focused on the variations in displacement in the canyon when $\theta = 0, \pi/6$, and $\pi/3$ (Section 3: Results and Discussion).

2.2. A 2-D model of symmetric canyon

Fig. 3 presents a schematic illustration showing a 2-D canyon, which is symmetrical along the *z*- axis, embedded within an elastic half-space on the *x*-*z* plane and excited by *P* waves. Symbols $2a$ and d in Fig. 3 respectively represent the width and depth of the symmetric canyon.